ELSEVIER

Journal of Photochemistry and Photobiology A: Chemistry 118 (1998) 173–181

Journal of Photochemistry and Photobiology A:Chemistry

Modelling intramolecular electron transfer reactions in cytochromes and in photosynthetic bacteria reaction centres

Luís G. Arnaut*, Sebastião J. Formosinho[1]

Chemistry Department, University of Coimbra, 3049, Coimbra Codex, Portugal

Received 5 May 1998; received in revised form 27 July 1998; accepted 4 August 1998

Abstract

Electron transfer rates within protein systems with various donor acceptor distances, reaction-free energies and temperatures, are calculated as the product of an electron tunneling probability and a nuclear distortion activation term. The electronic factor is given by the frequency of electronic motion in the donor, the donor electron energy, the donor–acceptor distance and the protein refractive index. Nuclear distortion is obtained from bond lengths, force constants and bond orders of the co-factor bonds involved in the reaction coordinate. The nuclear factor is calculated according to thermal activation and nuclear tunneling mechanisms. The calculation of distance, free-energy and temperature dependence of photoinduced-intraprotein electron transfer rates in Ru/Zn-modified cytochromes and myoglobins does not rely on fitting unknown parameters to kinetic data and is in good agreement with the experiment. Systems with reduced masses lower than 100 a.m.u. may undergo sizable nuclear tunneling at room temperature.

Keywords: Electron transfer reactions; Cytochromes; Photosynthetic reaction centres; Intersecting-state model

1. Introduction

Efficient long-distance electron transfer (ET) reactions are essential for biological processes such as photosynthesis and respiration. Significant advances in the understanding of such ETs have been achieved from systematic studies of photosynthetic ET chains in bacteria reaction centres (RCs) [1] and of photoinduced ET in ruthenium-modified cytochromes and myoglobins [2]. These intramolecular ET rates have been measured over a wide range of edge-to-edge donor–acceptor distances (3.8 Å $\leq r_e \leq$ 23 Å), reaction-free energies (15 kJ mol^{-1} $\geq \Delta G^0 \geq -150$ kJ mol^{-1}) and temperatures (5 K $\leq T \leq$ 330 K). Further developments in this field would benefit from simple theoretical models which estimate ET rate constants under these conditions without resorting to the fitting of parameters to the biological systems. The theoretical models presented here provide the basis for such predictions and rationalizations in biological ET reactions, and can be used to calculate absolute rates and their (distance, driving force, temperature) dependences in good agreement with experimental data on ruthenium-modified cytochromes, ruthenium/zinc-modified myoglobins and RCs.

We follow the intersecting-state model [3] to calculate intraprotein ET rate constants as the product of electronic and nuclear factors. The reactions considered in this work are non-adiabatic. In the electronically non-adiabatic limit, the effective electronic frequency for the transfer of an electron from the donor to the acceptor is much lower than the nuclear vibrational frequencies of the donor and acceptor reactive modes and the transition state for the ET reaction is formed many times before reactants are successfully converted to products. In this non-adiabatic limit the reaction frequency is controlled by the frequency of electronic motion in the donor, $\nu_{el} \approx 10^{15}$ s^{-1} [4], and by the exponential decay of the electronic factor with r_e. The coefficient (β) of this decay is controlled by the optical dielectric constant (ε_{op}) of the medium where the electronic wavefunction propagates [5]. The nuclear factor results from the rearrangement of donor and acceptor bonds from the equilibrium positions to their transition-state configurations. These nuclear configurational changes conserve the momentum and distance of the nuclei when the electron is transferred, but the configurations may not be intermediate between those of the oxidised and reduced forms of each reactant. The configurational changes are calculated from the bond lengths, force constants and bond orders of the

*Corresponding author.

[1]Also at Escola Superior de Ciências e Tecnologia, Universidade Católica Portuguesa, 3500 Viseu, Portugal.

1010-6030/98/$ – see front matter
PII: S1010-6030(98)00367-0

reactive bonds of electron donor and acceptor. The dissipation of the reaction energy may impose dynamic restrictions to the rates of very exothermic reactions ($\Delta G^0 < -50$ kJ mol^{-1}). This dissipation is promoted by the coupling between reactive and non-reactive modes, and is described by a dynamic parameter, Λ. The value, $\Lambda = 130$ kJ mol^{-1}, was obtained in the calculation of ET rates in RCs [4], and is assumed constant for the protein systems addressed in this study. Thus, the intraprotein ET rate constants calculated in this study do not involve the fitting of any new parameters to the kinetic data.

2. Theoretical models

2.1. Electronic factors

Two fundamentally different methodologies have been employed to interpret the distance dependence of ET reactions. One is to characterize a large variety of biological systems by a typical (empirical) square electron tunneling barrier and to assume that all ET rates in biological systems have the same exponential distance decay coefficients ($\beta \approx 1.4$ Å^{-1}) [6]. This 'homogeneous' barrier model found support in Dutton's compilation of the distance dependence of biological ETs [1] but was criticised on the basis of large deviations between predicted and observed rates in some ruthenium-modified cyt *c* [7]. The other strategy accounts for the detailed structure of the biological spacer between donor and acceptor, and calculates the most favourable pathways for electronic transmission [8]. This 'pathway' model has proved helpful in interpreting distance-dependent ETs on two-site fixed-distance donor–acceptor systems with a redox-active metal complex (usually a ruthenium complex) attached to the surface of a structurally characterized metalloprotein [9], but has failed to explain the insensitivity of ET rates in some site-directed protein mutants to changes in residues of the proposed electronic pathway [10] or the different pathway contributions in cyt *c* and Mb [11]. Furthermore, ad hoc arguments about the electronic mediation efficiency of particular H-bonds on special paths have to be invoked to reconcile the pathway model with distance-dependent ETs in azurin and myoglobins [12,13]. Refined versions of these models may lead to better estimates of the distance-dependent ET reactions in proteins. The 'homogeneous' barrier may be replaced by two of three types of barriers [14], related with different density regions or structural motifs (α helices or β sheets), at the cost of additional empirical parameters [15]. The 'relatively few pathways' may be complemented by multiple and nearly degenerate (hundreds of) pathways [11], at the cost of increased computational labour and loss of physical insight. However, the similar β values observed in very diverse media [5] are difficult to accommodate in these protein-tailored models.

The electron tunneling decay coefficients of ET reactions in methyltetrahydrofuran (MTHF) glass at 77 K range from $\beta = 1.10$ to 1.44 Å^{-1}, as the binding energy of the electron in the donor goes from 1.87 to 4.02 eV [16]. The binding energy is related to the energy cost of moving the electron from the donor to the lowest conduction state of the medium. According to the WKB approximation [17], the decay coefficient for electron tunneling through a square tunneling barrier of height Φ is

$$\beta = \frac{4\pi}{h}\sqrt{2m_e\Phi} = 1.025\sqrt{\Phi} \quad (1)$$

where m_e is the electron mass at rest and the constant is obtained when Φ is expressed in eV and β in Å^{-1}. Thus, $\beta = 1.10$ Å^{-1} should correspond to tunneling through a barrier of $\Phi = 1.15$ eV and $\beta = 1.44$ Å^{-1} should correspond to $\Phi = 1.97$ eV. The nearly constant ratio between binding energies and tunneling barriers for ET through MTHF glass, suggests that the former should be scaled by an approximately constant factor (1.6–2.0). In the STM experiment, on the other hand, ET from a platinum surface (work function $\Phi_0 = 5.03$ eV) to a tungsten tip ($\Phi_0 = 4.55$ eV) in the vacuum, yields a experimental decay coefficient $\beta = 2.17$ Å^{-1} [18,19] in agreement with the value calculated with Eq. (1), $\beta = 2.24$ Å^{-1}, using the average work functions of Pt and W. These data strongly suggest that the effective tunneling barrier is lower than the binding energy of the electron in the donor by a factor approaching the optical dielectric constant of the medium, $\varepsilon_{op} = {n_D}^2$ where n_D is the refractive index,

$$\Phi = \frac{\Phi_0}{\varepsilon_{op}} \quad (2)$$

This treatment was used to describe the distance dependence decay of ET reactions in diverse systems such as metal-monolayer-metal junctions, donor–acceptor systems dispersed in rigid organic glasses, intramolecular ET in rigid donor-bridge-acceptor species in solution and redox centres attached to electrodes through adsorbed monolayers [5].

We use the following argument to rationalize the fact that the electron tunneling barrier is not the difference between the energy of the electron in the lowest conduction state of the spacer and in the donor [3]. Let us call Φ_0 the energy of the electron in the donor relative to its energy at rest in the vacuum. The electron tunneling barrier through the vacuum will be Φ_0. Let us now suppose that the electron tunnels through a medium. If the conduction band of the medium is of much higher energy than the energy of the electron in the donor, the medium will behave like a dielectric. The separation of charges produces an electric field and, at the electronic frequency, the polarization of the dielectric reduces the magnitude of the electric field by the factor ε_{op}. The electric potential is also reduced by the same factor. Thus, the electron tunneling barrier through a dielectric is lower by a factor of ε_{op} than the barrier for tunneling through vacuum, as expressed by Eq. (2). We also expect that, when the energy of the conduction band of the medium approaches that of the electron in the donor, the medium tends to behave

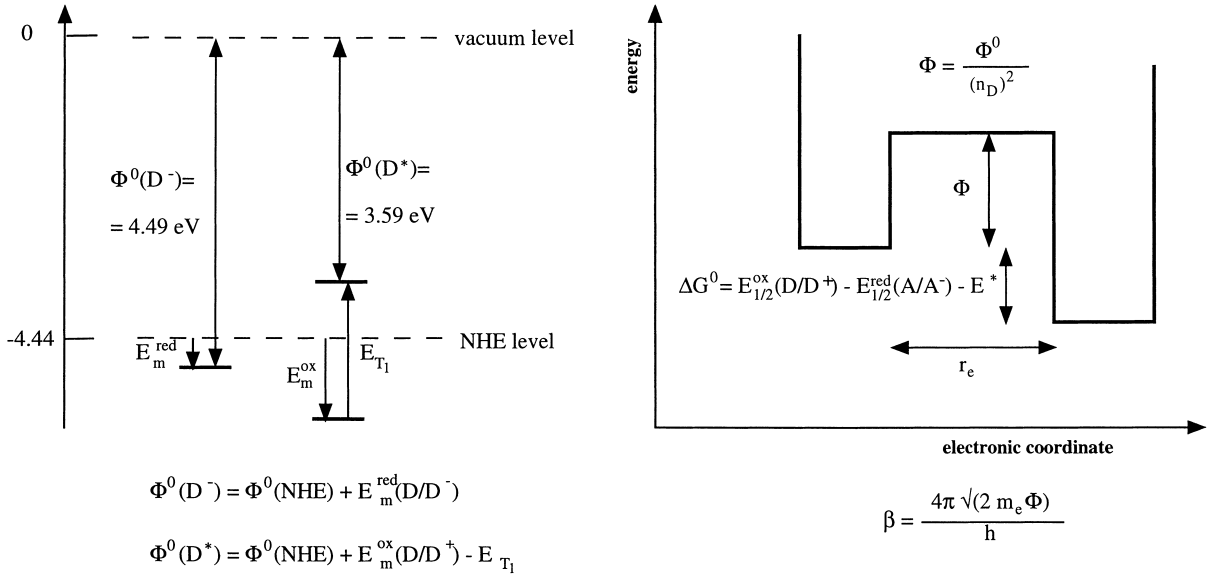

Fig. 1. Calculation of the electron tunneling decay coefficient, β, for an ET from Fe^{2+} cyt b_5 or from $(bpy)_2Ru^{2+}(Mebpy)^*$(Cys65) to an electron acceptor, as the WKB solution for the probability of tunneling through a square potential energy barrier; n_D is the refractive index, m_e is the electron mass at rest and r_e is the donor–acceptor edge-to-edge distance.

like an electric wire rather than as a dielectric, and the tunneling barrier follows the difference between the energy of the electron in conduction band and the donor.

Fig. 1 illustrates applications of our electron tunneling model to the intraprotein photoinduced ET $(bpy)_2Ru^{2+}(Mebpy)^*(Cys65) \rightarrow Fe^{3+}$ cyt b_5 and back recombination Fe^{2+} cyt $b_5 \rightarrow (Cys65)(Mebpy)Ru^{3+}(bpy)_2$. The tunneling barriers are not the same for the photoinduced forward and thermal reverse processes. The main features of our model are: (i) relating the energy of the electron in the donor to its energy at rest in the vacuum (Φ_0), using the electrochemical midpoint potential of the donor (E_m) and the absolute potential of NHE ($\Phi_{NHE} = 4.44$ eV) [20]; (ii) weighting the electron tunneling barrier by the optical dielectric constant of the intervening medium, Eq. (2); (iii) calculating the tunneling decay coefficients, Eq. (1), from the permeability of a square potential energy barrier to an electron impacting with a constant frequency (ν_{el}); (iv) calculating the reaction frequency of an electronically non-adiabatic ET as the product of a constant electronic frequency by the electronic permeability of the barrier [4]

$$\nu = \nu_{el} \exp(-\beta r_e) \quad (3)$$

We apply this model to ET in proteins using the literature values of E_m for each redox centre and the refractive index of formamide, $n_D \approx 1.45$ at room temperature, because ε_{op} of proteins was estimated to be close to that of amides [21]. We use experimental edge-to-edge donor–acceptor distances (r_e), defined as the distance between the carbon atom at the edge of the π-system of the donor in closest contact with that of the acceptor [22]. We assume that the frequency of electronic motion in the donor is constant and approaches $\nu_{el} = 10^{15}$ s^{-1}, which is a value commonly used for aromatic species. Actually, there is a reciprocal relation between the size of the donor and ν_{el} [5]. Taking r_e as the distance from the centre of the σ bond of the donor to the centre of the acceptor attachment bond [23], assumes a larger size for the donor and, consequently, requires a lower ν_{el} [5].

For cytochromes and myoglobins with known E_m and r_e, making $n_D \approx 1.45$ and $\nu_{el} = 10^{15}$ s^{-1} as in our previous application of the electron tunneling model to RCs, it is possible to estimate *absolute* distance-dependent non-adiabatic factors at room temperature. The density of the medium (and consequently the external temperature and pressure) can be related to β through n_D.

This model may be refined to include anisotropy of ε_{op} in a protein. In the physically meaningful limits of $\varepsilon_{op} = 1.88$ (*n*-hexane, representing aliphatic residues) and 2.24 (benzene, representing aromatic residues), with $\Phi_0 = 4$ eV we obtain $\beta = 1.50$ $Å^{-1}$ and 1.37 $Å^{-1}$, respectively. Only in such extreme limits does this sophistication of the model become as important as accounting for the electron–donor energy. For example, the 'special pair' (P) of bacteriochlorophyll molecules in *Rhodobacter* (Rb.) *sphaeroides* RC has $E_m = 0.50$ eV and an electronic excited-state energy $E^* = 1.39$ eV, thus $\Phi_0 = -3.55$ eV with $\varepsilon_{op} = 2.1$, gives $\beta = 1.33$ $Å^{-1}$; however, the primary ubiquinone acceptor (Q_A) of this RC has $E_m = -0.05$ eV; thus $\Phi_0 = 4.39$ eV and $\beta = 1.48$ $Å^{-1}$.

It is possible to relate the dependence of the electron tunneling barrier on ε_{op} with its dependence on atom density between the pairs of redox centers. Typical ET proteins have mean atom densities around 70%. This density increases up to 75–79% in azurin and plastocyanin, and attains a maximum of about 88% in the region between Q_A and second ubiquinone (Q_B) of the RC [15]. Protein regions with higher-

than-average atom densities should have a lower barrier to electron tunneling than normal protein regions. They do display slightly accelerated experimental ET rates (usually a factor of 3 or less [15]). We can have a rough idea of the influence of density variations in the value of ε_{op} considering that organic solvents have thermal expansion coefficients ca. $1.2 \times 10^{-3}\ K^{-1}$ and that the typical temperature dependence of their n_D values ranges from -0.00035 to $-0.00055\ K^{-1}$. Thus, a 15% volume change corresponds to an increase of n_D by 0.056. A similar n_D increase in the region between Q_A and Q_B relative to normal protein regions, leads to $\varepsilon_{op} = 2.268$ and $\beta = 1.43\ Å^{-1}$. Given that r_e between Q_A and Q_B is 13.5 Å, this decrease in β with an increase in density corresponds to an ET rate increase by a factor of 2.

2.2. Nuclear factors

A complete treatment of the ET rates must also account for the Franck–Condon factors of electron donors and acceptors. According to the Marcus theory [24], the Franck–Condon factors arise from two sources: geometric differences between the redox centres in their oxidised and reduced states, and reorganisation of the medium surrounding the redox centers. In the Marcus theory, the internal reorganization energy of the redox centres is proportional to $(l_{ox}–l_{red})^2$, where l_{ox} (l_{red}) is the metal–ligand bond length with the metal in the oxidised (reduced) state. The medium is described by a dielectric continuum characterized by its bulk optical (ε_{op}) and static (ε_s) dielectric constants, and its repolarization energy is considered to be proportional to $(1/\varepsilon_{op} - 1/\varepsilon_s)\,(1/2a_1 + 1/2a_2 - 1/r_c)$ where r_c is the distance between the centres of the two (spherical) reactants of radii a_1 and a_2. For example, polypyridine ruthenium and iron complexes like $Fe(phen)_3^{2+/3+}$ (phen = 1,10-phenanthroline) or $Ru(bpy)_3^{2+/3+}$ (bpy = 2,2′-bipyridine), which are low-spin complexes in both oxidation states with $l_{ox} \approx l_{red}$, are calculated to have zero internal reorganization energy and a medium reorganization energy of $\lambda = 0.57$ eV in water [25]. In view of the small structural differences between oxidised and reduced cytochromes ($l_{ox} \approx l_{red}$) [26,27], and of their much larger diameters than polypyridine complexes (26 Å vs. 13.6 Å), a straightforward application of the Marcus theory predicts a reorganization energy of cyt *c* in water ca. 0.30 eV. In fact, the temperature dependence of the cyt *c* and cyt b_5 self-exchanges gives $\lambda = 0.72$ and 1.2 eV, respectively [28]. In order to reconcile the theory with the experimental values, Marcus and Sutin estimated λ of cyt *c* using $a = 5$ Å, $r_c = 18$ Å and $\varepsilon_s = 10$ [24]. The geometric parameters have a poor correspondence with the actual physical system and ε_s is much larger than the value obtained from a microscopic treatment of the cyt *c*, $\varepsilon_s = 2.9$ [29].

The difficulties of conventional ET theories in calculating absolute nuclear reorganization energies in biological systems lead many authors to obtain relative estimates of such reorganization energies using the Marcus additivity relation [24]. According to this, the cross-exchange reorganization energy λ_{12} is the average of the two complementary self-exchange reorganization energies (λ_{11} and λ_{22}). Thus, the self-exchange rate of a cytochrome can be calculated from the cross-reaction rates involving the cytochrome and redox partners with known self-exchange rates. Intramolecular ET rates in ruthenium-modified cytochromes provide a consistent ground to calculate relative ET rates. The rates of $Ru^{II}L(im)(His33)–Fe^{III}$cyt *c* reactions (L = phen, bpy or bpy-methylated derivatives, and im = imidazole), yield $\lambda_{12} = 0.74$ eV [30]. Using $\lambda_{22} = 0.57$ eV for $Ru(bpy)_3^{2+/3+}$, we obtain $\lambda_{11} = 0.91$ eV for cyt *c*. A similar study with $Ru^{II}L_3(His33)–Fe^{III}$cyt b_5 (L = bpy or methylated derivatives) gave $\lambda_{12} = 0.87$ eV [31], i.e. $\lambda_{11} = 1.17$ eV for cyt b_5. Cytochromes have consistently larger reorganization energies than polypyridine ruthenium and iron complexes in spite of their much larger diameters and comparable differences between the oxidised and reduced structures. Furthermore, binding cyt *c* to cyt b_5 and consequent exclusion of water from the binding domain, does not change the reorganization energy of cyt b_5 [31]. This is additional evidence in favour of the view that dielectric continuum models overestimate medium reorganization energies and that the internal modes are the major contributors to the Franck–Condon factors [3,4,32]. The solvent contribution to the reorganization energy of blue copper proteins was also considered negligible [33]. Thus, biological ET reactions call for an alternative model to calculate Franck–Condon factors.

We have found that the intersecting-state model, ISM [34] is appropriate to calculate the nuclear energy barrier of ET reactions involving transition-metal complexes [35,36], organic species in solution [32] and photosynthetic bacteria RCs [4]. According to ISM, the dominant contributions to the reaction coordinate come from the bonds where the electron is located in both reactants, i.e., the metal–ligand bonds in metal complexes or the conjugated bonds of aromatic systems in organic species. The reaction coordinate is defined as the sum of the bond length changes of the *j* reactive bonds from their equilibrium positions in the reactants to their configuration in the transition state, $d = |l_1^{\ddagger} - l_{1,eq}| + |l_2^{\ddagger} - l_{2,eq}| + \ldots + |l_j^{\ddagger} - l_{j,eq}|$. The reaction coordinate *d* is related to the equilibrium bond lengths (long bonds are more prone to change than short bonds) and bond orders (single bonds distort more easily than double bonds). A simple expression for *d* is obtained assuming that the overall bond order of reactants and products is conserved in an isothermic ET process [3]

$$d_0 = \left[\frac{l_{ox,r} + l_{red,r}}{2} + \frac{l_{red,p} + l_{ox,p}}{2}\right]\left[\frac{a' \ln(2)}{n^{\ddagger}}\right] \quad (4)$$

where $a' = 0.156$ is a constant related to Pauling's 'universal' constant [37], and $n^{\ddagger}$ actually represents the transition-state bond order of the reactive bonds because higher energy electronic configurations may mix extensively with

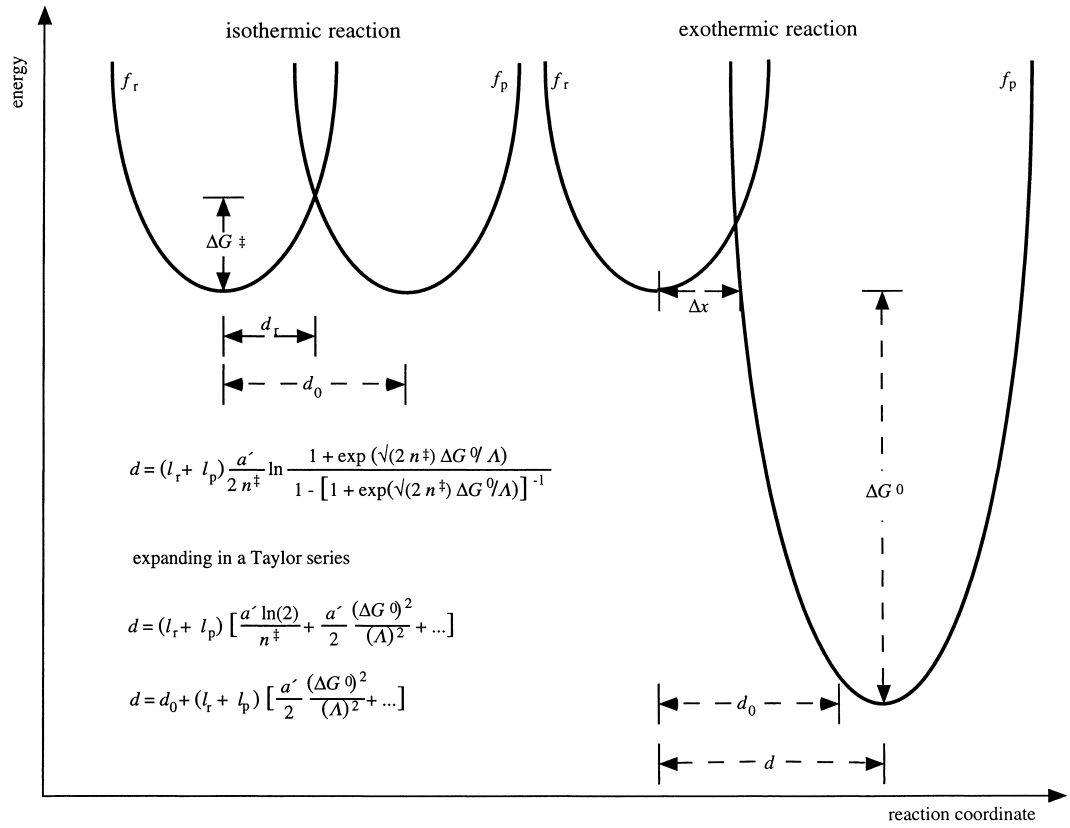

Fig. 2. Free-energy profiles along the reaction coordinates defined by ISM for isothermic and exothermic reactions. In the first case the reaction coordinate is d_0 whereas for the second case it also depends on ΔG^0 and on the coupling between reactive and non-reactive modes (Λ). For very strongly coupled modes (high Λ), the reaction energy is efficiently dissipated and $d \approx d_0$. The nuclear tunneling barrier width is represented by Δx.

the valence-bond descriptions at the transition state and increase the valence bond order. The conservation of the bond order leads to $(n^{\ddagger})^{-1} = (2n_r^{\ddagger})^{-1} + (2n_p^{\ddagger})^{-1}$, with $n_r^{\ddagger} = (n_{ox,r}^{\ddagger} + n_{red,r}^{\ddagger})/2$. When more than one bond of the oxidised reactant (reduced product) is involved in the reaction coordinate, $l_{ox,r}$ ($l_{red,p}$) is taken as the average of all the relevant bonds lengths. The same is valid for the reduced reactant (oxidised product). Using the relations shown in Fig. 2, we obtain the nuclear reorganization free-energy barrier

$$\Delta G^{\ddagger} = \frac{1}{2}\left(\frac{f_{ox,r} + f_{red,r}}{2}\right) d_r^2 \tag{5}$$

where $f_{ox,r}$ ($f_{red,r}$) is the oxidised (reduced) reactant force constant. The force constants of reactant organic molecules are taken from the normal-coordinate analysis of their vibrational spectra and $f_{ox,r}$ ($f_{red,r}$) is the average of the force constants of the reactive bonds. The metal–ligand force constants of metal complexes are estimated from $f_{MLi} = (\nu_{MLi}/\nu_{MLref})^2 f_{MLref}$, where ν_{MLi} and ν_{MLref} are the metal–ligand vibrational frequencies of the complex and of a reference with known metal–ligand force constants, f_{MLref}. Depending on the complex, the references used were $Ru(bpy)_3^{2+}$ [38] or Ni^{II} porphine [39]. The i metal–ligand bonds in a metal complex behave as local modes; thus, the effective metal-complex force constant in the oxidized state is $f_{ox}{}^2 = f_{ox,1}{}^2 + f_{ox,2}{}^2 + \cdots + f_{ox,i}{}^2$ [3]. The same is assumed for the reduced state.

The dissipation of the reaction energy in very exothermic ($\Delta G^0 < -50$ kJ mol^{-1}) ETs may impose dynamical restrictions on the reaction rates. Such restrictions increase with the weakness of the coupling between reactive and non-reactive modes. ISM introduces a coupling parameter (Λ) to account for this effect in the reaction coordinate. Weak coupling (low Λ) enhances the reactive bond length changes, as shown in Fig. 2. This figure presents the complete equation of the ISM reaction coordinate [3,34,40],

$$d = \left[\frac{l_{ox,r} + l_{red,r}}{2} + \frac{l_{red,p} + l_{ox,p}}{2}\right]\frac{a'}{2n^{\ddagger}} \times \ln\left\{\frac{1 + \exp\left(\sqrt{2n^{\ddagger}}\Delta G^0/\Lambda\right)}{1 - \left[1 + \exp\left(\sqrt{2n^{\ddagger}}\Delta G^0/\Lambda\right)\right]^{-1}}\right\} \tag{6}$$

valid for all values of ΔG^0, and its expansion in a Taylor series.

ISM is particularly well suited to calculate biological ET rates because it uses readily available structural, electronic and spectroscopic data on the redox centers and a value of Λ that is transferable from model systems. Intramolecular ETs

Table 1
Reactive bond parameters employed in the calculation of Franck–Condon factors of ET reactions in cytochromes and RCs

	f_{red} (10^3 kJ mol^{-1} Å^{-2})	f_{ox} (10^3 kJ mol^{-1} Å^{-2})	$l_{red}+l_{ox}$ (Å)	$n^{\ddagger}$	μ (a.m.u.)	Reference
$Ru^{2+/3+}$–NH_3	1.23	1.52	4.26	1.25[a]	14	[35]
$Ru^{2+/3+}$–N(bpy)	1.32	1.32	4.09	2[b]	14	[38]
$Fe^{2+/3+}$–N(histidine)[c]	1.44	1.42	3.97[d]	2[b]	14	[35]
$Fe^{2+/3+}$–N(pyrrole)[e]	1.0	1.0	4.12[d]	2[b]	14	
$Fe^{2+/3+}$–S(methionine)	1.44	1.44	4.59[d]	1.60[a]	14	[41]
$Mg^{2+/3+}$–N(aromatic)	0.56	0.56	4.00	2[b]	14	[4]
2,2′-Bipyridine	3.76	3.76	2.78	1.44	37	[42]
Porphine	3.69	3.69	2.79	1.36	74	[39]
Bacteriochlorin	3.43	3.43	2.83	1.31	74	[43]

[a]Using the equation of Gordy, Pauling's electronegativities and the force constants, bond lengths and $n^{\ddagger}=1$ of $Fe(OH_2)_6^{2+/3+}$ as in [35].
[b]This enhanced transition-state bond order is due to the mixing of higher energy resonance structures at the transition state [35].
[c]Assumed to be identical to the Fe–N bonds of $Fe(phen)_3^{2+/3+}$.
[d]From the metal–ligand bond lengths of tuna cyt *c* [26,27].
[e]Assumed to have the same force constant as the Ni–N bonds of Ni^{II}porphine [39].

in solution have Λ in the range 100–140 kJ mol^{-1} [5]. ETs in RCs have been described with $\Lambda \approx 130$ kJ mol^{-1} [4]. In this work we use the data in Table 1, the experimental ΔG^0 values and $\Lambda = 130$ kJ mol^{-1} to calculate the nuclear reorganization energies ($\Delta G^{\ddagger}$) of the ruthenium-modified cytochromes ruthenium/zinc-modified cytochromes and RCs. We calculate the thermally activated intramolecular ET rate constants from

$$k_{ta} = \nu_{el}\exp(-\beta r_e)\exp\left(-\Delta G^{\ddagger}/RT\right) \quad (7)$$

Thus, for weakly exothermic reactions ($|\Delta G^0| < 50$ kJ mol^{-1}) *our rate constant calculations do not involve any fitting* to experimental rates of the biological systems. For more exothermic reactions our calculations make use of an empirical parameter ($\Lambda = 130$ kJ mol^{-1}), that was not fitted to the kinetic data presented in this work and appears to be typical of ET reactions in biological systems.

3. Results and discussion

3.1. Distance effects

Ruthenium-modified cytochromes have been extensively used to test ET theories. The experimental data presently available cover a wide range of donor–acceptor distances and reaction-free energies. Fig. 3(A) compares the calculated and experimental distance dependence of $(NH_3)_5Ru^{II}$-(HisX)–Fe^{III}cyt *c* → $(NH_3)_5Ru^{III}$(HisX)–Fe^{II}cyt *c* ETs [44–46] and $Ru^{III}(bpy)_2$(im)(HisX)–Fe^{II}cyt *c* → $Ru^{II}(bpy)_2$(im)-(HisX)–Fe^{III}cyt *c* [7,10,47]. The intercepts of the lines reveal the different Franck–Condon factors of these reactions which were included in the calculations. The force constants, bond lengths and bond orders employed are reported in the figure captions and were obtained exclusively from the data in Table 1, by strict application of the criteria discussed above. This is also valid for Figs. 4–6. Variations in the force constants are compensated by concomitant variations in the bond lengths. The calculated rates do have a steep dependence on $n^{\ddagger}$ [3]. The reported edge-to-edge distances of His79, His72 [7] and His47 [44] were measured to the

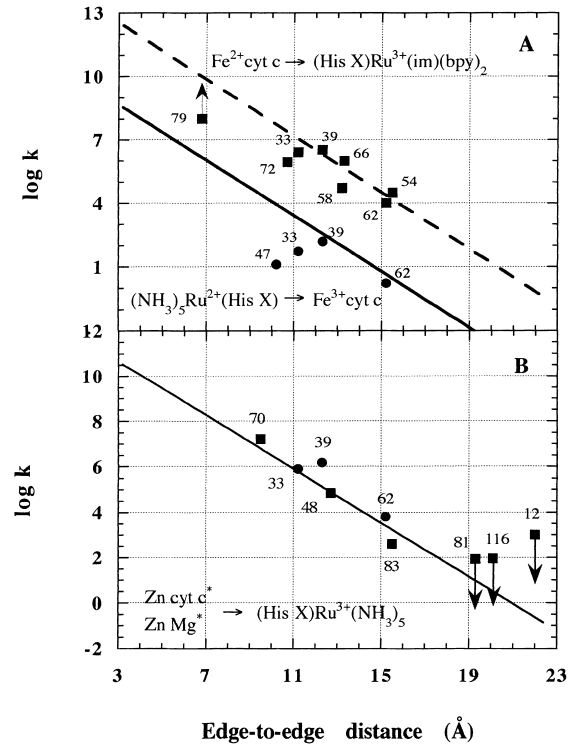

Fig. 3. Distance dependence of intramolecular ETs. (A) $(NH_3)_5Ru^{II}$-(HisX)–Fe^{III}cyt *c*: ■ [44–46] and ——— ($f_r = 2.95 \times 10^3$ kJ mol^{-1} Å^{-2}, $f_p = 3.25 \times 10^3$ kJ mol^{-1} Å^{-2}, $l_r + l_p = 4.20$ Å, $n^{\ddagger} = 1.61$, $\Delta G^0 = -0.13$ eV, $\Phi_0 = 4.52$ eV); $Ru^{III}(bpy)_2$(im)(HisX)–Fe^{II}cyt *c*: ● [7,10,47] and - - - ($f_r = f_p = 3.04 \times 10^3$ kJ mol^{-1} Å^{-2}, $l_r + l_p = 4.13$ Å, $n^{\ddagger} = 1.96$, $\Delta G^0 = -0.8$ eV, $\Phi_0 = 4.7$ eV). (B) $(NH_3)_5Ru^{III}$(HisX)–Zn cyt* *c*: ● [48]; $(NH_3)_5Ru^{III}$(HisX)–Zn Mb*: ■ [11,49]; the line was calculated with $f_r = 3.67 \times 10^3$ kJ mol^{-1}Å^{-2}, $f_p = 3.37 \times 10^3$ kJ mol^{-1} Å^{-2}, $l_r + l_p = 3.51$ Å, $n^{\ddagger} = 1.37$, $\Delta G^0 = -0.8$ eV, $\Phi_0 = 3.7$ eV.

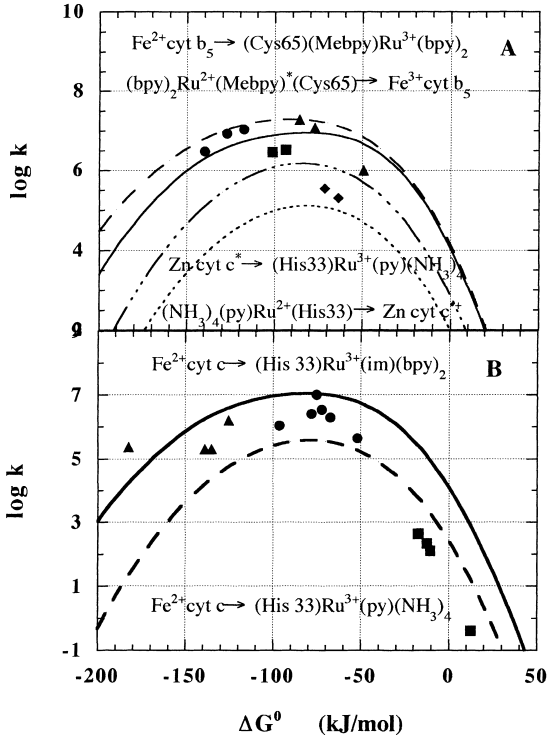

Fig. 4. Free-energy dependence of intramolecular ETs. (A) RuL_2(Mebpy)(Cys65)cyt b_5 where L = bpy, substituted-bpy [31]; the transfers from cyt b_5 to Ru^{3+} are represented by ● and - - - ($f_r = f_p = 3.04 \times 10^3$ kJ mol^{-1} Å^{-2}, $l_r + l_p = 4.08$ Å, $n^{\ddagger} = 2.00$, $r_e = 12$ Å, $\Phi_0 = 4.39$ eV), and the transfers from the diimine π^* orbital of the ruthenium complex to cyt b_5 are represented by ▲ and ——— ($f_r = f_p = 3.30 \times 10^3$ kJ mol^{-1} Å^{-2}, $l_r + l_p = 3.43$ Å, $n^{\ddagger} = 1.67$, $r_e = 12$ Å, $\Phi_0 = 3.88$ eV). $(NH_3)_4$Ru(L)(His33)Zn cyt c where L = pyridine, isonicotinamide [50]; the transfers from the pyrrole ring π^* orbital to Ru^{3+} are represented by ■ and the – · – ($f_r = 3.63 \times 10^3$ kJ mol^{-1} Å^{-2}, $f_p = 3.39 \times 10^3$ kJ mol^{-1} Å^{-2}, $l_r + l_p = 3.50$ Å, $n^{\ddagger} = 1.43$, $r_e = 11.2$ Å, $\Phi_0 = 3.82$ eV), and the transfers from Ru^{2+} to Zn cyt $c^{\cdot+}$ are represented by ◆ and by the · · · ($f_r = 3.39 \times 10^3$ kJ mol^{-1} Å^{-2}, $f_p = 3.63 \times 10^3$ kJ mol^{-1} Å^{-2}, $l_r + l_p = 3.50$ Å, $n^{\ddagger} = 1.43$, $r_e = 11.2$ Å, $\Phi_0 = 4.52$ eV). (B) RuL_2(Y)(His33)cyt c where L = phen, bpy, substituted-bpy, and Y = imidazole, CN [30]; transfers from cyt c to Ru^{3+}: ● and ——— ($f_r = f_p = 3.04 \times 10^3$ kJ mol^{-1} Å^{-2}, $l_r + l_p = 4.13$ Å, $n^{\ddagger} = 1.96$, $r_e = 11.2$ Å, $\Phi_0 = 4.70$ eV); transfers from the diimine π^* orbital of the ruthenium complex to cyt c: ▲; $(NH_3)_4$Ru(L)(His33)cyt c where L = NH_3, pyridine, *cis*- and *trans*-isonicotinamide [46]: ■ and - - - ($f_r = 3.21 \times 10^3$ kJ mol^{-1} Å^{-2}, $f_p = 2.97 \times 10^3$ kJ mol^{-1} Å^{-2}, $l_r + l_p = 4.19$ Å, $n^{\ddagger} = 1.69$, $r_e = 11.6$ Å, $\Phi_0 = 4.70$ eV).

methionine sulfur atom complexed to the iron ion. To these distances we added the typical Fe–S bond length of cytochromes (2.3 Å), because S and Fe are weakly coupled.

Fig. 3(B) shows the distance dependence of $(NH_3)_5Ru^{III}$-(HisX)–Zn cyt* $c \rightarrow (NH_3)_5Ru^{II}$(HisX)–Zn cyt$^{\cdot+}$ c [48] and $(NH_3)_5Ru^{III}$(HisX)–Zn Mb* $\rightarrow (NH_3)_5Ru^{II}$(HisX)–Zn Mb$^{\cdot+}$ [11,49] photoinduced ETs. These systems have identical Franck–Condon factors because the electron donor is the electronically excited porphyrin. The experimental values of His12Mb, His116Mb and His81Mb are upper limits to the true intramolecular ET rate due to the presence of unresolved bimolecular contributions to the observed rate [11].

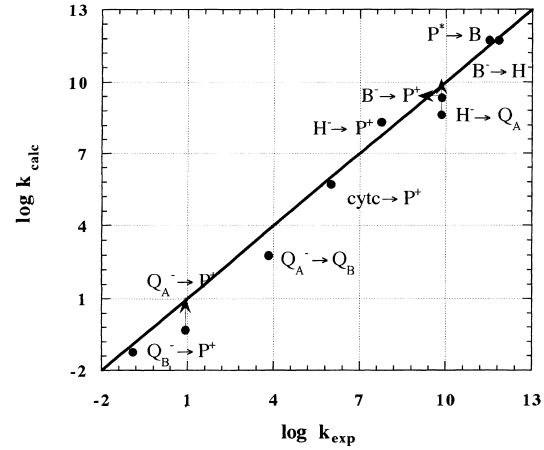

Fig. 5. Comparison between experimental and calculated ET rates in *Rb. sphaeroides* RCs. The edge-to-edge distances, reaction-free energies and references to the experimental rates are as follows. Excited special pair (P^*) → accessory bacteriochlorophyll (B_L): 4.7 Å, −0.04 eV, ref. [51]; $B_L^{\cdot-}$ → bacteriopheophytin (H_L): 3.8 Å, −0.21 eV, ref. [51]; $H_L^{\cdot-}$ → primary quinone acceptor (Q_A): 9.0 Å, −0.65 eV, ref. [51]; $Q_A^{\cdot-}$ → Q_B: 13.5 Å, −0.06 eV, ref. [52]; $B_L^{\cdot-}$ → oxidized special pair ($P^{\cdot+}$): 3.8 Å, −1.35 eV, from the >99% charge separation efficiency; $H_L^{\cdot-}$ → $P^{\cdot+}$: 10.0 Å, −1.14 eV, ref. [53]; $Q_A^{\cdot-}$ → $P^{\cdot+}$: 21.5 Å, −0.49 eV, ref. [54]; $Q_B^{\cdot-}$ → $P^{\cdot+}$: 22.5 Å, −0.43 eV, ref. [55]; cyt c_2 → $P^{\cdot+}$: 10.0 Å, −0.16 eV, ref. [56]. The parameters involved in the calculations were obtained from the data in Table 1 [4]. Only lower limits are calculated for the $H_L^{\cdot-}$ → Q_A and $Q_A^{\cdot-}$ → $P^{\cdot+}$ rates because the native ubiquinone-10 has a long isoprenoid tail that accelerates these rates [54] and this was not included in the calculations.

3.2. Free-energy effects

The photoinduced ETs in L_2Ru^{II}(Mebpy)*(Cys65)–Fe^{III}-cyt $b_5 \rightarrow L_2Ru^{II}$(Mebpy)$^{\cdot+}$(Cis65)–$Fe^{II}$cyt b_5 where L = bpy, Me_2bpy or bpym [31], do not have the same

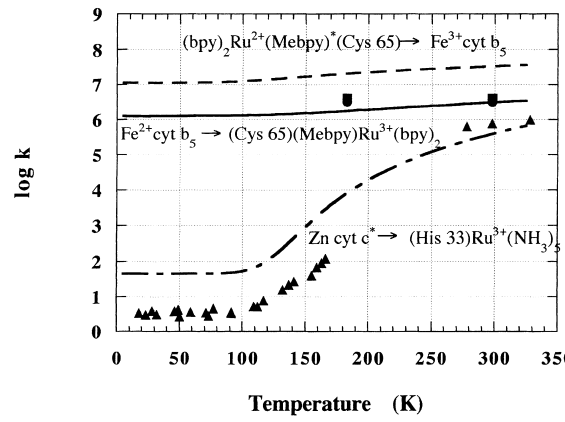

Fig. 6. Temperature dependence of intramolecular ETs. $(bpy)_2Ru^{II}$(Mebpy)*(Cis65)–Fe^{III}cyt b_5: ■ [58] and - - - ($f_r = f_p = 3.30 \times 10^3$ kJ mol^{-1} Å^{-2}, $l_r + l_p = 3.43$ Å, $n^{\ddagger} = 1.67$, $\Delta G^0 = -0.80$ eV, $r_e = 12$ Å, $\Phi_0 = 3.59$ eV, $m = 97$ a.m.u.); $(bpy)_2Ru^{III}$(Mebpy)(Cis65)–Fe^{II}cyt b_5: ● [58] and - - - ($f_r = f_p = 3.04 \times 10^3$ kJ mol^{-1} Å^{-2}, $l_r + l_p = 4.08$ Å, $n^{\ddagger} = 2.00$, $\Delta G^0 = -0.05$ eV, $r_e = 12$ Å, $\Phi_0 = 4.39$ eV, $m = 56$ a.m.u.); $(NH_3)_5$-Ru^{III}(HisX)–Zn cyt* c: ▲ [59,60] and – · – line ($f_r = 3.67 \times 10^3$ kJ mol^{-1} Å^{-2}, $f_p = 3.37 \times 10^3$ kJ mol^{-1} Å^{-2}, $l_r + l_p = 3.51$ Å, $n^{\ddagger} = 1.37$, $\Delta G^0 = -0.70$ eV, $r_e = 11.2$ Å, $\Phi_0 = 3.82$ eV, $m = 242$ a.m.u.).

Franck–Condon factors as the corresponding thermal reactions. The cyt b_5 contribution is given by its four Fe–N(pyrrole) and two Fe–N(histidine) bonds, all having $n^{\ddagger} = 2$, but the other reactant is either the electronically excited bpy or the ruthenium–ligand bonds. The Franck–Condon and non-adiabatic factors of photoinduced and thermal reactions give comparable rates and the data are not widely dispersed (Fig. 4(A)). The same figure also shows the free-energy dependence of photoinduced $L(NH_3)_4Ru^{III}$(His33)–Zn cyt* $c \rightarrow L(NH_3)_4Ru^{II}$(His33)–Zn cyt$^{\bullet+}$ c and thermal $L(NH_3)_4Ru^{II}$(His33)–Zn cyt$^{\bullet+}$ $c \rightarrow L(NH_3)_4Ru^{III}$(His33)–Zn cyt c processes, L = pyridine or isonicotinamide [50].

Fig. 4(B) illustrates the consequences of the different Franck–Condon factors associated with the (His33)$Ru^{3+/2+}$(py)$(NH_3)_4$ and (His33)$Ru^{3+/2+}L_2$ redox centres, where L = bpy, phen, CN or imidazole [30], because the other redox partner is always cyt c, with its four Fe–N(pyrrole), one Fe–N(histidine) and one Fe–S(methionine) bonds. Heterogeneous Franck–Condon factors influence the series of thermal and photoinduced reactions shown in the upper part of this figure. In particular, when the donor electron is in the diimine π^{*} orbital, the rates in the inverted region are predicted to be faster than when it is in the metal–ligand orbitals. We only show the calculations using the thermal reaction coordinate. The photoinduced reactions are likely to have enhanced r_e values. The most exothermic reactions may lead to the ferrohaem metal-to-ligand charge-transfer state ($\approx$101 kJ mol^{-1}) [30].

The distance and free-energy dependences of the ET rates in *Rb. sphaeroides* RCs can be calculated using the edge-to-edge distances between the co-factors [1,22], the free-energy change of each ET reaction [4], the data in Table 1 for the co-factors and the models described above. We have systematically used $n_D = 1.45$ for the protein and $\Lambda = 130$ kJ mol^{-1} for the coupling between the modes. No parameters are fitted in the calculations presented in Fig. 5. The calculated $Q_A^{\bullet-} \rightarrow Q_B$ rate is 10 times lower than the experimental one. Part of this difference is due to the use of $\varepsilon_{op} = 2.1$ in a region where ε_{op} should approach 2.3, for the reasons discussed above.

3.3. Temperature effects

For sufficiently low temperatures, nuclear tunneling becomes the dominant reaction mechanism. Its contribution to the observed rate can be calculated using the same barrier as for thermal reaction. The nuclear tunneling probability for the type of barriers shown in Fig. 2 is given by the WKB solution to a triangular barrier [4,57], yielding the nuclear tunneling rate

$$k_{tu} = \nu_{el}\exp(-\beta r_e)\frac{1}{1+\exp\left[2\frac{\pi}{h}(2\mu\,\Delta E^{\ddagger})^{1/2}\Delta x\right]} \quad (8)$$

where $\Delta E^{\ddagger} \approx \Delta G^{\ddagger}$, Δx is the width of the tunneling barrier and the reduced mass of the system is determined by the assumption that the oxidised and reduced reactants have common $\Delta E^{\ddagger}$ and Δx values, $\sqrt{\mu} = \sqrt{\mu_{ox}} + \sqrt{\mu_{red}}$. The normal mode analysis of each organic reactant suggests that its effective reduced mass is the sum of the reduced masses of the different independent oscillators in the reactant, i.e. porphyrins: $\mu_{ox} = 8\mu_{CC} + 4\mu_{CN}$. The local mode description of each metal complex implies that the independent ligand atoms vibrate against a still center of mass, and its effective reduced mass is that of the ligand atom, i.e. cyt c: $\mu_{ox} = (5m_N + m_S)/6$.

Fig. 6 shows the temperature dependence of photoinduced $(bpy)_2Ru^{II}$(Mebpy)*(Cis65)–Fe^{III}cyt $b_5 \rightarrow (bpy)_2Ru^{II}$(Mebpy)$^{\bullet+}$(Cis65)–$Fe^{II}$cyt b_5 and back-recombination $(bpy)_2Ru^{III}$(Mebpy)(Cis65)–Fe^{II}cyt $b_5 \rightarrow (bpy)_2Ru^{II}$(Mebpy)(Cis65)–$Fe^{III}$cyt b_5 [58], as well as photoinduced $(NH_3)_5Ru^{III}$(HisX)–Zn cyt* $c \rightarrow (NH_3)_5Ru^{II}$(HisX)–Zn cyt$^{\bullet+}$ c [59,60]. In the latter system we added the atomic mass of zinc (65.4 a.m.u.) to the reduced mass of the porphyrin (74 a.m.u.), because the Zn–cyt complex is not planar and the zinc atom is likely to be displaced in the ET process. It is clear that nuclear tunneling gives a sizable contribution to the room temperature rates of the first systems, but only becomes relevant ca. 120 K for the latter one. This difference is due to the high reduced mass of the Zn–cyt complex. Similar results have been obtained in the description of the reduction of the 'special pair' by cyt c_2 in *Chromatium vinosum* RCs [4,61].

4. Conclusions

Our analysis of a large number of ET reactions in cytochromes, zinc–porphyrin derivatives of myoglobins and RCs shows that both electronic and nuclear factors are important in determining biological ET rates. The electronic factor has an exponential dependence on the edge-to-edge distance between donor and acceptor. The distance decay coefficients have only a mild dependence on the details of the protein structure separating donor and acceptor, but are significantly dependent on the energy of the electron in the donor. The nuclear factor can be calculated from structural and electronic parameters of the reactants and products. The contribution of the medium to the reorganization energy of the ET process is much smaller than that of the reactants. This, however, is not related to a specific ability of the protein medium to lower reorganization energies and accelerate ET reactions. Rather, it is a general phenomenon also apparent in electron self-exchanges in solution.

The weak temperature dependence of some ET rates arises from appreciable nuclear tunneling contributions, even at room temperature. A tunnel effect theory, originally developed to calculate rates of radiationless transitions, provides a quantitative account of the observed temperature dependences.

The theoretical analysis developed in this work can be extended to other biological electron carriers and provides a

non-empirical approach to such ET reactions. Furthermore, it provides an adequate theoretical understanding of these systems and may guide the design of new synthetic systems aimed at the conversion of light into chemical energy.

Acknowledgements

The authors thank Junta Nacional de Investigação Científica and Praxis XXI Programme (European Union) for financial support; project no. PRAXIS/2/2.1/QUI/390/94.

References

[1] C.C. Moser, J.M. Keske, K. Warncke, R.S. Farid, P.L. Dutton, Nature 355 (1992) 796.
[2] H.B. Gray, J.R. Winkler, Annu. Rev. Biochem. 65 (1996) 537.
[3] S.J. Formosinho, L.G. Arnaut, R. Fausto, Prog. Reaction Kinetics 23 (1998) 1.
[4] L.G. Arnaut, S.J. Formosinho, J. Photochem. Photobiol. A: Chem. 111 (1997) 111.
[5] L.G. Arnaut, L.G. Formosinho, J. Photochem. Photobiol. A: Chem. 100 (1996) 15.
[6] J.J. Hopfield, Proc. Natl. Acad. Sci. U.S.A. 71 (1974) 3640.
[7] D.S. Wuttke, M.J. Bjerrum, I.-J. Chang, J.R. Winkler, H.B. Gray, Biochim. Biophys. Acta 1101 (1992) 168.
[8] D.N. Beratan, J.N. Betts, J.N. Onuchic, Science 252 (1991) 1285.
[9] D.S. Wuttke, M.J. Bjerrum, J.R. Winkler, H.B. Gray, Science 256 (1992) 1007.
[10] D.R. Casimiro, J.H. Richards, J.R. Winkler, H.B. Gray, J. Phys. Chem. 97 (1993) 13073.
[11] D.R. Casimiro, L.-L. Wong, J.L. Colón, T.E. Zewert, J.H. Richards, I.-J. Chang, J.R. Winkler, H.B. Gray, J. Am. Chem. Soc. 115 (1993) 1485.
[12] J.R. Winkler, H.B. Gray, J. Biol. Inorg. Chem. 2 (1997) 399.
[13] R.J.P. Williams, J. Biol. Inorg. Chem. 2 (1997) 373.
[14] C.C. Moser, C.C. Page, R. Farid, P.L. Dutton, J. Bioenerg. Biomembr 27 (1995) 263.
[15] C.C. Moser, C.C. Page, X. Chen, P.L. Dutton, J. Biol. Inorg. Chem. 2 (1997) 393.
[16] V.V. Krongauz, J. Phys. Chem. 96 (1992) 2609.
[17] R.P. Bell, The Tunnel Effect in Chemistry, Chapman and Hall, London, 1980, pp 39.
[18] G. Binnig, H. Rohrer, C. Gerber, E. Weibel, Physica, 109/110B (1982) 2075.
[19] G. Binnig, H. Rohrer, Ang. Chem. Int. Ed. Engl. 26 (1987) 606.
[20] S. Trasatti, Pure Appl. Chem. 58 (1986) 955.
[21] L.I. Krishtalik, Biochim. Biophys. Acta 977 (1989) 200.
[22] J. Deisenhofer, O. Epp, I. Sinning, H. Michel, J. Mol. Biol. 246 (1995) 429.
[23] G.L. Closs, L.T. Calcaterra, N.J. Green, K.W. Penfield, J.R. Miller, J. Phys. Chem. 90 (1986) 3673.
[24] R.A. Marcus, N. Sutin, Biochim. Biophys. Acta 811 (1985) 265.
[25] N. Sutin, Acc. Chem. Res. 15 (1982) 275.
[26] T. Takano, R.E. Dickerson, J. Mol. Biol. 153 (1981) 79.
[27] T. Takano, R.E. Dickerson, J. Mol. Biol. 153 (1981) 95.
[28] D.W. Dixon, X. Hong, S.E. Woehler, A.G. Mauk, B.P. Sishta, J. Am. Chem. Soc. 112 (1990) 1082.
[29] I. Muegge, P.X. Qi, A.J. Wand, Z.T. Chu, A. Warshel, J. Phys. Chem. B 101 (1997) 825.
[30] G.A. Mines, M.J. Bjerrum, M.G. Hill, D.R. Casimiro, I.-J. Chang, J.R. Winkler, H.B. Gray, J. Am. Chem. Soc. 118 (1996) 1961.
[31] J.R. Scott, M. McLean, S.G. Sligar, B. Durham, F. Millett, J. Am. Chem. Soc. 116 (1994) 7356.
[32] S.J. Formosinho, L.G. Arnaut, Bull. Chem. Soc. Jpn. 70 (1997) 977.
[33] S. Larsson, A. Broo, L. Sjölin, J. Phys. Chem. 99 (1995) 4860.
[34] A.J.C. Varandas, S.J. Formosinho, J. Chem. Soc., Faraday Trans. 2 82 (1986) 953.
[35] S.J. Formosinho, L.G. Arnaut, J. Mol. Struct. (Theochem.) 130 (1994) 105.
[36] S.J. Formosinho, L.G. Arnaut, J. Photochem. Photobiol. A: Chem. 82 (1994) 11.
[37] L. Pauling, J. Am. Chem. Soc. 69 (1947) 542.
[38] D.P. Strommen, P.K. Mallick, G.D. Danzer, R.S. Lumpkin, J.R. Kincaid, J. Phys. Chem. 94 (1990) 1357.
[39] X.-Y. Li, R.S. Czernuszewicz, J.R. Kincaid, Y.O. Su, T.G. Spiro, J. Phys. Chem. 94 (1990) 31.
[40] S.J. Formosinho, in: S.J. Formosinho, I.G. Csizmadia, L.G. Arnaut, (Eds.), Theoretical and Computational Models for Organic Chemistry, NATO ASI, Kluwer, Dordrecht, 1991, pp 159.
[41] S. Hu, J.R. Kincaid, J. Am. Chem. Soc. 113 (1991) 9760.
[42] N. Neto, M. Muniz-Miranda, L. Angeloni, E. Castellucci, Spectrochim. Acta, Part A 39A (1982) 97.
[43] C.-Y. Lin, T.G. Spiro, J. Phys. Chem. 101 (1997) 472.
[44] P. Osvath, G.A. Salmon, A.G. Sykes, J. Am. Chem. Soc. 110 (1988) 7114.
[45] B.E. Bowler, T.J. Meade, S.L. Mayo, J.H. Richards, H.B. Gray, J. Am. Chem. Soc. 111 (1989) 8757.
[46] J. Sun, J.F. Wishart, M.B. Gardineer, M.P. Cho, S.S. Isied, Inorg. Chem. 34 (1995) 3301.
[47] M.J. Bjerrum, D.R. Casimiro, I.-J. Chang, A.J. Di Bilio, H.B. Gray, M.G. Hill, R. Langen, G.A. Mines, L.K. Skov, J.R. Winkler, D.S. Wuttke, J. Bioenerg. Biomemb. 27 (1995) 295.
[48] J.R. Winkler, H.B. Gray, Chem. Rev. 92 (1992) 369.
[49] A.W. Axup, M. Albin, S.L. Mayo, R.J. Crutchley, H.B. Gray, J. Am. Chem. Soc. 110 (1988) 435.
[50] T.J. Meade, H.B. Gray, J.R. Winkler, J. Am. Chem. Soc. 111 (1989) 4353.
[51] A.R. Holzwarth, M.G. Müller, Biochemistry 35 (1996) 11820.
[52] R.J. Debus, G. Feher, M.Y. Okamura, Biochemistry 25 (1986) 2276.
[53] A. Ogrodnik, M. Volk, R. Letterer, R. Feick, M.E. Michel-Beyerle, Biochim. Biophys. Acta 936 (1988) 361.
[54] M.R. Gunner, D.E. Robertson, P.L. Dutton, J. Phys. Chem. 90 (1986) 3783.
[55] A. Labahan, J.M. Bruce, M.Y. Okamura, G. Feher, Chem. Phys. 197 (1995) 355.
[56] X. Lin, J.C. Williams, J.P. Allen, P. Mathis, Biochemistry 33 (1994) 13517.
[57] S.J. Formosinho, L.G. Arnaut, Adv. Photochem. 16 (1991) 67.
[58] J.R. Scott, A. Willie, M. McLean, P.S. Stayton, S.G. Slogar, B. Durham, F. Millett, J. Am. Chem. Soc. 115 (1993) 6820.
[59] H. Elias, M.H. Chou, J.R. Winkler, J. Am. Chem. Soc. 110 (1988) 429.
[60] L.-H. Zang, A.H. Maki, J. Am. Chem. Soc. 112 (1990) 4346.
[61] D. DeVault, J.H. Parkes, B. Chance, Nature 215 (1967) 642.